

System-Theoretic Analysis and Least-Squares Design of Microfluidic Channels for Flow-Induced Molecular Communication

A. Ozan Bicen, *Student Member, IEEE*, and Ian F. Akyildiz, *Fellow, IEEE*

Abstract—Flow-induced Molecular Communication (FMC), where molecular transport is performed via flow, is utilized in microfluidic channels to enhance diffusion-based molecular communication. The incorporation of the microfluidic channel and the transport of molecules by flow, i.e., convection, require a rigorous analysis to develop an end-to-end concentration propagation model and a design for microfluidic channels. To the best of our knowledge, this is the first attempt to analyze concentration propagation in microfluidic channels from FMC perspective and devise them specifically to enhance the FMC. In this paper, a system-theoretic analysis of molecular transport is presented first. The system-theoretic model incorporates the solution of flow velocity in microfluidic channels and yields an end-to-end transfer function for concentration propagation based on building blocks of microfluidic channels. Then, the design of microfluidic channels is performed based on the least-squares Finite Impulse Response (FIR) filtering to achieve the desired end-to-end transfer function in FMC. According to the desired pass and stop bands, the required length and aspect-ratio parameters of the microfluidic channels are obtained for FIR filtering. The transfer functions for FMC is elaborated via numerical results. Furthermore, two example designs of microfluidic channels are presented for least-squares FIR band-pass and band-stop filtering in FMC.

Index Terms—Least-squares linear filtering, microfluidics, molecular communication, nano communications, systems theory.

I. INTRODUCTION

MOLECULAR COMMUNICATION (MC) is one of the fundamental approaches towards enabling biocompatible nano communication networks. In the literature, there exists different molecular communication options, such as time of arrival, number and type of molecules for information encoding, and chemotaxis of bacteria, active transport using molecular motors, and ion channels for signal propagation [1]–[3]. In this paper, we target the MC based on utilization of the concentration of molecules as information carrying signal. The concentration of molecules is transmitted, i.e., released, into the fluidic

Manuscript received January 22, 2013; revised May 05, 2013 and July 16, 2013; accepted July 17, 2013. Date of publication July 26, 2013; date of current version September 06, 2013. The associate editor coordinating the review of this manuscript and approving it for publication was Prof. Eduard Axel Jorswieck. This work was supported by the U.S. National Science Foundation (NSF) by Grant CNS-1110947.

The authors are with the Broadband Wireless Networking Laboratory (BWN-Lab), School of Electrical and Computer Engineering, Georgia Institute of Technology, Atlanta, GA 30332 USA (e-mail: bozan@ece.gatech.edu; ian@ece.gatech.edu).

Color versions of one or more of the figures in this paper are available online at <http://ieeexplore.ieee.org>.

Digital Object Identifier 10.1109/TSP.2013.2274959

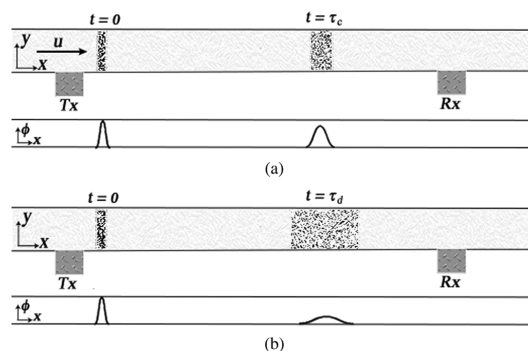


Fig. 1. Propagation of the concentration signal from the transmitter (Tx) to the receiver (Rx) patch through the microfluidic channel based on the convection (a) and the diffusion (b). At an arbitrary position, the propagation time of convection based transport with flow velocity u is much less than diffusion based transport, i.e., $\tau_d \gg \tau_c$, which alleviates dispersion of molecules in (a) compared to (b).

channel and is propagated, i.e., transported, to the receiver. According to the received concentration of molecules, the receiver performs the desired chemical reaction, such as synthesis of molecules or light emission. The diffusion-based MC has been a focus of interest in the research world so far, in which molecules are transported solely by diffusion through the fluid medium [4]. The released molecule concentration sustains attenuation, i.e., dispersion, and the delay inside the fluid while diffusing towards the receiver. However, the transport of molecules can be enhanced via flow, i.e., convection, to mitigate dispersion and delay. The transport of molecules inside microfluidic channel is illustrated in Fig. 1(a) and (b) for the convection and the diffusion, respectively. Furthermore, the convection can be guided through a confined fluid medium such as a microchannel, i.e., microfluidic channel. Microfluidics describes fluid dynamics at submillimeter-scale. The basic idea of microfluidics is to integrate chemical assay and molecular biology operations, such as detection and separation, on one chip [5], [6]. Microfluidic channels and flow can jointly provide control over propagation of molecules from transmitter to the receiver in MC. Here, we focus on the communication between transmitter and receiver placed in a microfluidic channel in which the fluid flows which constitutes a new MC paradigm, i.e., the Flow-induced Molecular Communications (FMC).

In FMC, the fluid flowing through a microfluidic channel serves as a communication channel and connects patches of molecular transmitter and receiver, such as bacterial habitat [7]. A basic MC scheme over microfluidic channel is presented in

Fig. 1(a) where the convection provides transport of released molecules by the transmitter to the receiver over a microfluidic channel. Overall, FMC brings significant advantages over traditional MC, including utilization of flow for enhancing molecular transport and guiding concentration propagation via the microfluidic channel. FMC can be used to provide nano communications for a very wide range of emerging applications, specifically in nanomedicine, medical microbiology, and immediate point-of-care testing of samples for biochemical toxins and dangerous pathogens. However, the realization of these envisioned applications depends on an accurate analysis and efficient design of microfluidic channels for FMC.

For the realization of FMC, it is imperative to develop new and efficient communication techniques. The challenges and requirements to be addressed for the analysis and design of microfluidic channels for FMC can be summarized as follows:

- *Modeling the Molecular Transport via Flow inside Microfluidic Channels:* The concentration propagation inside the microfluidic channels must be investigated from the FMC perspective. The solution of the flow rate inside the microfluidic channels must be determined, and the microfluidic channel configurations must be studied to understand the propagation of transmitted molecules.
- *Enhancing the Concentration Propagation via Microfluidic Channel Design:* The shape of microfluidic channels must be optimized to alleviate the dispersion and the delay between the transmitter and the receiver. The microfluidic channel parameters, i.e., length and cross-section, must be adjusted to enhance the FMC via filtering spectrum of the concentration signal.

All these challenges coupled with the physical limitations of microfluidic channels, immediate diagnosis and treatment requirements for mission critical clinical applications call for a thorough analysis and efficient design of FMC to realize nano communications in bio-compatible environments. So far, to the best of our knowledge, there is no prior work on analytical modeling of concentration propagation and design of microfluidic channels from the FMC point of view.

While a channel model solely based on diffusion is proposed in [4], the analysis of noise sources and the communication capacity in diffusion-based concentration propagation have been the main approaches for molecular communication research [3], [8]–[12]. Recently, modeling and simulation of concentration propagation in microfluidic channels have been a field of interest [13]–[19]. While these studies on microfluidics have been adequate for the analysis of separation, dispersion, and the generation of concentration profiles via microfluidic devices, they do not focus on the communication perspective, which requires the propagation characteristics of the FMC channel to be revealed based on the transmitted concentration signal and the channel parameters. Furthermore, the microfluidics has been considered for networking of lab-on-a-chip systems [20], where possible different configurations of microfluidic technologies are surveyed for droplet-based nano communication. Overall, the incorporation of convection and the inherited features from microfluidics require a new analysis for an accurate and efficient development of communication techniques and design of microfluidic channels.

In this paper, first, system-theoretic analysis of the FMC is performed which provides a framework to determine the end-to-end concentration propagation in microfluidic channels based on flow velocity and channel configurations, i.e., straight, turning, and interconnections. Then, the least-squares design of microfluidic channels is presented in which physical parameters of microfluidic channels, i.e., interconnection, cross-section and length, are optimized to obtain desired transfer function at the receiver via Finite Impulse Response (FIR) filtering. To the best of our knowledge, this is the first work on the FMC focusing on the analysis and design of microfluidic channels for end-to-end concentration propagation and finite impulse filtering, respectively. The distinctive features of our paper are as follows:

- 1) **A Flow Model in Microfluidic Channels:** A contemporary overview of fluid flow inside microfluidic channels is presented, and a general technique for deriving flow rate in microfluidic channels is developed. This technique is used to determine the flow rate inside a specific channel for a given microfluidic channel topology.
- 2) **An End-to-end Concentration Propagation Model:** The molecular transport models are developed by incorporating convection to reveal the attenuation, delay, and the transfer function for the basic microfluidic channel and the interconnection configurations. Using systems theory, the end-to-end concentration propagation model is presented for FMC.
- 3) *Design of Microfluidic Channels for FIR Filtering:* To enhance the end-to-end FMC, an FIR filtering structure is developed based on the microfluidic channels. For a desired frequency response, the FIR filter coefficients are optimized via least-squares method. The obtained filter coefficients are mapped to transfer function of individual microfluidic channels to determine the length and aspect-ratio.

The remainder of this paper is organized as follows. In Section II, the characteristics of fluid flow in microfluidic channels and the lumped parameter model is introduced. The analysis of molecular transport in microfluidic channels via flow is presented in Section III. Building blocks of microfluidic channels are analyzed for concentration propagation and end-to-end concentration propagation model is presented in Section IV for each building block, as well as for the overall end-to-end model. In Section V, the design of microfluidic channels for finite impulse filtering via least-squares is presented. Numerical results are presented in Section VI. Finally, the paper is concluded in Section VII.

II. FLUID FLOW MODEL

To understand and work with the microfluidic channels, the hydrodynamic behavior of fluids in microchannels must be first understood. Here, we provide a comprehensive look at the physical phenomena of the fluid flow inside microfluidic channels and how it makes the utilization of convection for FMC possible.

The Navier-Stokes equation relating the velocity field \mathbf{u} of the fluid flow to pressure p under the constant density ρ , constant

viscosity μ , and conservation of mass ($\nabla \cdot \mathbf{u} = 0$) assumptions is as

$$\rho \left(\frac{\partial \mathbf{u}}{\partial t} + (\mathbf{u} \cdot \nabla) \mathbf{u} \right) = -\nabla p + \mu \nabla^2 \mathbf{u} + \mathbf{F} \quad (1)$$

where \mathbf{F} represents the body forces. We assume there is no electrical field acting on the fluid, and the gravitational body force diminishes due to the hydrostatic pressure gradient [21]. The density ρ of a liquid is in the order of $\approx 10^3 \text{ kg/m}^3$ which is comparable to a solid's density for many practical purposes [21]. Therefore, the fluid flows, such as water and aqueous solutions, are well approximated as incompressible, i.e., constant density ρ , in microfluidic channels [22].

To guide design of microfluidic channels for FMC, Navier-Stokes equation is solved analytically in the particular cases. Specifically, the simplification of the Navier-Stokes equation is performed under unidirectional flow through an infinite channel assumption, where the fluid velocity field and the velocity field gradient are orthogonal, i.e., $(\mathbf{u} \cdot \nabla) \mathbf{u} = 0$. Fluid flow is said to be laminar under this condition, and the total flow is formed by the addition of contribution from each lamina. In the following subsections, the fluid flow characteristics and the solution steps of the fluid flow rate for given microfluidic channels are presented.

A. Characteristics of Flow in Microfluidic Channels

The Reynolds number (Re), which gives the relative importance of inertial and viscous forces, is used to characterize laminar flow in microfluidic channels and is defined as [21]

$$\text{Re} \triangleq \frac{\rho u D_H}{\mu} \approx \frac{\text{inertial forces}}{\text{viscous forces}} \quad (2)$$

where μ is the viscosity, D_H is the hydraulic diameter of the channel, and u is the characteristic area-averaged velocity depending on the volumetric flow rate Q of the fluid and cross-section area A of the channel. D_H is given by

$$D_H = \frac{4A}{\chi} \quad (3)$$

where χ is the perimeter of the channel. In a circular cross-section channel with radius r , $D_H = 2r$ and $u = Q/(\pi r^2)$. For a square channel with the width w , $D_H = w$ and $u = Q/w^2$. For a rectangular channel with width much greater than height, i.e., $w \gg h$, $D_H = 2w$ and $u = Q/(wh)$.

In the laminar flow case, i.e., at small Reynolds numbers ($\text{Re} < 2300$) for the smooth channels, the viscous forces are large enough to overcome the inertial forces and to keep the fluid in line and prevent random rapid fluctuations of the fluid [23]. The fluid flows in microchannels are almost always at low Reynolds number, i.e., $\text{Re} < 1$, due to small hydraulic diameters D_H and relatively slow volumetric flow rates Q . Furthermore, in microfluidic channels the inertial effects such as gravity, and turbulence are negligible [24]–[26]. The laminar flow and the absence of turbulence are essential to minimize unsteady-state flows at turning channels and connection nodes in microfluidic channels [27]. Moreover, when the distance l from the inlet of a channel with radius r satisfies the condition $l/r \gg \text{Re}$, the laminar flow can be taken as fully-developed, and analysis of

infinite channels can be used to analyze flows in finite length channels [21], [22].

B. Poiseuille Flow

Poiseuille flow is the solution of steady laminar flow in microfluidic channels [21], [22]. Flow in microfluidic channels is defined by perturbation or superposition of Poiseuille flow. In a Poiseuille flow, the flow is driven by pressure, i.e., pressure difference causes the flow, unidirectional, i.e., through only single direction and orthogonal to other axes, and taken to be in steady-state, i.e., there is no acceleration of the fluid [21].

The channel is taken to be parallel to x axis, and its cross-section is invariant. Using the steady flow ($\partial \mathbf{u}/\partial t = 0$), unidirectional velocity field ($u_y = u_z = 0$), fully developed laminar flow ($\partial u_x/\partial x = 0$), and smooth channel ($(\mathbf{u} \cdot \nabla) \mathbf{u} = 0$) assumptions, Navier-Stokes equation (1) is simplified as

$$\partial_x p(x) = \mu (\partial_y^2 + \partial_z^2) u_x(y, z) \quad (4)$$

where $u_x(y, z)$ is the only non-zero component of fluid velocity field which is independent of position in x direction and changes based on position in y , and z directions. Furthermore, since velocity field in y , and z directions are zero, the pressure drops in y and z directions are 0. Therefore, due to the constant pressure gradient in the x direction in (4), the pressure difference Δp between the two ends of the microfluidic channel is a linear function of x as

$$p(x) = p(x_0) - \frac{\Delta p}{l}(x - x_0) \quad (5)$$

where Δp is equal to $p(l) - p(x_0)$. Replacing (5) into (4), we obtain

$$(\partial_y^2 + \partial_z^2) u_x(y, z) = -\frac{\Delta p}{\mu l} \quad (6)$$

The flow velocity field is taken as zero at the boundaries of the channel, i.e., no-slip boundary condition is employed [21]. The flow in microfluidic channels is characterized by a parabolic velocity field, and the velocity of flow increases towards the center of the channel from the boundaries. The analytic solution of (6) for a rectangular cross-section channel, i.e., u_x^{rect} , is as [21]

$$u_x^{\text{rect}}(y, z) = \frac{4h^2 \Delta p}{\pi^3 \mu l} \sum_{n=1,3,5,\dots}^{\infty} \frac{1}{n^3} \left[1 - \frac{\cosh\left(\frac{n\pi y}{h}\right)}{\cosh\left(\frac{n\pi w}{2h}\right)} \right] \sin\left(\frac{n\pi z}{h}\right) \quad (7)$$

where h and w are the height and width of the microfluidic channel, respectively. For an elliptical cross-section, analytic solution of (6), i.e., u_x^{elps} , is found as [21]

$$u_x^{\text{elps}}(y, z) = \frac{\Delta p(a^2 b^2)}{2\mu l(a^2 + b^2)} \left(1 - \frac{y^2}{a^2} - \frac{z^2}{b^2} \right) \quad (8)$$

To have an accurate analysis and prosperous design of microfluidic channels, disruption of laminar flow should be prevented. For low Reynolds numbers, i.e. $\text{Re} < 1$, which is typical in microfluidic channels, fluid flow is not exposed to lateral mixing, i.e., turbulence, in turning channels. Due to vis-

ous forces, velocity field gradients in the direction of the axial direction is prevented, i.e., $(\mathbf{u} \cdot \nabla)\mathbf{u} = 0$, and laminar flow is conserved for turning microfluidic channel [28], [29].

C. Volumetric Flow Rate

Using flow velocity solutions of microchannels, volumetric flow rate Q can be determined as

$$Q \triangleq \int_S u_x(y, z) dy dz \quad (9)$$

where S is the area of the cross-section of the microfluidic channel. Therefore, to get the volumetric flow rate in the rectangular channel n , i.e., Q_n^{rect} , we need to spatially integrate the velocity contributions (7) of each lamina as

$$\begin{aligned} Q_n^{\text{rect}} &= \int_0^{w_n} \int_0^{h_n} u_x^{\text{rect}}(y, z) dz dy \\ &= \frac{8h_n^3 w_n}{\pi^4 \mu l_n} \sum_{i=1,3,5,\dots}^{\infty} \left[\frac{1}{i^4} - \frac{2h_n}{\pi w_n i^5} \tanh\left(\frac{i\pi w_n}{2h_n}\right) \right] \Delta p_n \end{aligned} \quad (10)$$

Using $\sum_{i=1,3,5,\dots}^{\infty} \frac{1}{i^4} = \pi^4/96$, and for channels with $w \gg h$ using $\tanh(\infty) = 1$, Q_n^{rect} in (10) can be further simplified as [21]

$$Q_n^{\text{rect}} \approx \frac{h_n^3 w_n}{12\mu l_n} \left(1 - 0.630 \frac{h_n}{w_n}\right) \Delta p_n \quad (11)$$

Furthermore, flow rate in square channels can easily be obtained via setting $h = w$ as

$$Q_n^{\text{sqre}} \approx 0.370 \frac{h_n^4}{12\mu l_n} \Delta p_n \quad (12)$$

However, due to assumption of $w \gg h$ for approximation, flow rate calculations for square channels exposed to error about 13%, while as the w/h ratio increases, this error diminishes, such as for $w/h = 2$ error is about 0.2% [21].

For the elliptical cross-section channel, flow rate is formulated via integration over an elliptically shaped cross-section with major axis radius a and minor axis radius b as

$$\begin{aligned} Q_n^{\text{elps}} &= \int_{-a_n}^{a_n} \int_{-b_n \sqrt{1-x^2/a_n^2}}^{b_n \sqrt{1-x^2/a_n^2}} u_x^{\text{elps}}(y, z) dy dz \\ &= \frac{\pi}{4\mu l_n} \frac{a_n^3 b_n^3}{a_n^2 + b_n^2} \Delta p_n \end{aligned} \quad (13)$$

Flow rate for a circular cross-section with radius a can be obtained via setting radius $r = b = a$ in (13) as

$$Q_n^{\text{circ}} = \frac{\pi r_n^4}{8\mu l_n} \Delta p_n \quad (14)$$

It is shown that for Poiseuille flow in microfluidic channels, there exists a linear relationship between volumetric flow rate Q and pressure drop Δp across the channel. This result is called

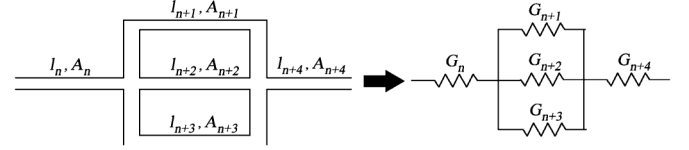


Fig. 2. Hydraulic conductance model.

TABLE I
SUMMARY OF HYDRAULIC CONDUCTANCE FOR DIFFERENT MICROCHANNEL CROSS-SECTIONS

Cross-section	Hydraulic Conductance
Rectangular (G_n^{rect})	$\frac{h_n^3 w_n}{12\mu l_n} \left(1 - 0.630 \frac{h_n}{w_n}\right)$
Square (G_n^{sqre})	$0.370 \frac{h_n^4}{12\mu l_n}$
Elliptical (G_n^{elps})	$\frac{\pi}{4\mu l_n} \frac{a_n^3 b_n^3}{a_n^2 + b_n^2}$
Circular (G_n^{circ})	$\frac{\pi r_n^4}{8\mu l_n}$

Poiseuille-Hagen law and will be used to develop equivalent circuit theory for flow modeling in FMC.

D. Hydraulic Conductance and Equivalent Circuit Theory

So far, the calculation of the average flow rate in microfluidic channels is presented. In (11), (12), (13), and (14), for a pressure drop of Δp across the microfluidic channel, a constant flow rate Q is found. This linear relationship yields well-known circuit theory analysis tools applicable to microfluidic channels. The linear relation between flow in the channel and pressure drop across channel, i.e., Hagen-Poiseuille law, is given as

$$Q = G \Delta p \quad (15)$$

where G is the hydraulic conductance of the microfluidic channel. Equivalent circuit representation of microfluidic channels is depicted in Fig. 2. The hydraulic conductances of various cross-sections is presented in the Table I. For the high aspect ratio rectangular channels, i.e., $h/w \rightarrow 0$, the hydraulic conductance of a channel becomes $G_n^{\text{rect}} = h_n^3 w_n / (12\mu l_n)$.

For low Re numbers in microfluidics, the addition of two finite length channels with different cross-section are shown to be still following the Poiseuille flow definition, i.e., non-accelerating and laminar flow [13], [21]. Therefore, Hagen-Poiseuille law can still be applied, and equivalent conductance of the series added channels can be calculated using circuit theory as

$$\begin{aligned} G_{\text{eq}} &= \frac{1}{\frac{1}{G_1} + \frac{1}{G_2} + \dots + \frac{1}{G_N}} \\ &= \frac{\prod_{n=1}^N G_n}{\sum_{n=1}^N \prod_{i=1, i \neq n}^N G_i} \end{aligned} \quad (16)$$

where G_n is the conductance of channel n with length l_n , width w_n , and height h_n , i.e., $G_n = G(l_n, w_n, h_n)$. The equivalent

conductance for parallel connected microfluidic channels can be obtained as

$$\begin{aligned} G_{\text{eq}} &= G_1 + G_2 + \cdots + G_N \\ &= \sum_{n=1}^N G_n \end{aligned} \quad (17)$$

For serial and parallel channels, the flow rate can be obtained from total pressure drop across the channels using (15). Furthermore, since the pressure drop across all parallel connected channels are the same by circuit theory, the total flow is divided among parallel sub-branches directly proportional to hydraulic conductance, as

$$Q_n = \frac{G_n}{G_{\text{eq}}} Q_+ \quad (18)$$

where Q_+ is the entering total flow rate to parallel branches. Moreover, hydraulic resistance of turning microchannels is shown to be equal to the one of the straight channel with the same cross-section and length [28], [29].

Here, we complete the lumped parameter modeling of flow rate in microfluidic channels. The microfluidic channels are modeled by hydraulic conductance based on the linear relation between the flow rate inside and the pressure drop across the channel. In the next subsection, the solution for flow velocity at each channel is formulated by utilizing the presented equivalent circuit model.

E. Analysis of Microfluidic Circuits for Flow Velocity

To analyze the microfluidic circuit, we use nodal formulation. A conservation of flow equation, i.e., KCL equation, is written for each node, where microfluidic channel n connects two nodes. There exists one KCL equation for each node k . In matrix form, nodal equations are represented as

$$\mathbf{G}\mathbf{p} = \mathbf{Q}_s \quad (19)$$

where $\mathbf{p} = [p_1, p_2, \dots, p_K]^T$ for a microfluidic circuit of K nodes, entries of matrix \mathbf{G} are the conductance between two nodes that are connected via single channel, and \mathbf{Q}_s represents the sum of entering flow from flow sources to node k .

When \mathbf{p} is determined, pressure drop across microchannels $\Delta\mathbf{p}$ is determined via the node-to-branch matrix \mathbf{B} as

$$\Delta\mathbf{p} = \mathbf{B}\mathbf{p} \quad (20)$$

where \mathbf{B} is an N -by- K matrix containing two entries of valued 1 with opposite signs at each row, which indicate pressure at which nodes should be subtracted to calculate pressure drop Δp_n for channel n . Then, multiplying pressure drop with hydraulic conductance of channels, flow rate across channels is found as

$$\mathbf{Q} = \mathbf{G}_c \Delta\mathbf{p} \quad (21)$$

where $\mathbf{Q} = [Q_1, Q_2, \dots, Q_N]$ with Q_n is the flow rate in channel n , and \mathbf{G}_c is a diagonal matrix with entries G_n for $n = 1, \dots, N$.

Finally, area-averaged velocity u of fluid is obtained via dividing volumetric flow rate Q by cross-section area A of the microfluidic channels as

$$\mathbf{u} = \mathbf{A}^{-1} \mathbf{Q} \quad (22)$$

where $\mathbf{u} = [u_1, u_2, \dots, u_N]$ with u_n is the area-averaged flow velocity in channel n , and \mathbf{A}^{-1} is a diagonal matrix whose entries are reciprocal of channel cross-section area, i.e., $A_n^{-1} = 1/A_n$. Next, molecular transport analysis is conducted by incorporating flow velocity model tailored for FMC.

III. MOLECULAR TRANSPORT ANALYSIS

Molecules are subject to the convection-diffusion through the microfluidic channels with the effect of flow. We assume there is no existing concentration in the channel, i.e., system is at rest. Molecules are released to or collected from the microfluidic channels by molecular transmitter and receiver, respectively. Here, we, first, formulate impulse response, transfer function, and delay of the concentration propagation through microfluidic channels for the FMC. Then, we investigate the duality of time-invariant and transnational-invariant properties of concentration propagation.

A. Impulse Response

The convection-diffusion equation is used to define behavior of mass transport inside flowing fluid. It is a linear partial differential equation defined as

$$\frac{\partial \phi}{\partial t} = -u \nabla \phi + D \nabla^2 \phi \quad (23)$$

where D is the diffusion constant adjusted based on the cross-section parameters of the microfluidic channel due to the Taylor dispersion [30]. The convection-diffusion equation relates to the change of concentration ϕ in time on the left hand side, i.e., $\partial \phi / \partial t$, to convection ($u \nabla \phi$) and diffusion ($D \nabla^2 \phi$) terms on the right hand side. Due to linearity property, solution for end-to-end concentration propagation can be written as linear combination of propagation in building blocks, such as straight and turning channels, and interconnections.

In Section II, it is shown that fluid flow is unidirectional and is in x direction in microfluidic channels. Therefore, the concentration is invariant in the other directions. To analyze the molecular transport in microfluidic channels, the one-dimensional solution of convection-diffusion in the direction of flow, i.e., x , is sufficient to capture the convection-driven transport of molecules [13]–[17]. The finite amount of concentration injected ϕ into the flow in microfluidic channel at an instant t_0 by a point source located at x_0 can be modeled as an impulse using the Dirac delta function δ as

$$\phi(x, t) = \frac{M}{A} \delta(x - x_0, t - t_0) \quad (24)$$

where M is the amount of the mass, and A is the cross-section area, then M/A gives the mass per unit area. For a unity concentration, i.e., $M/A = 1$, response to such an input, i.e., impulse response, is obtained as [21]

$$h(x, t) = \frac{1}{\sqrt{4\pi D(t-t_0)}} \exp\left(-\frac{(x - (x_0 + u(t-t_0)))^2}{4D(t-t_0)}\right) \quad (25)$$

Defining $l = x - x_0$, and $\tau = t - t_0$, impulse response becomes

$$h(l, \tau) = \frac{1}{\sqrt{4\pi D\tau}} \exp\left(-\frac{(l - u\tau)^2}{4D\tau}\right) \quad (26)$$

B. Transfer Function

The frequency response of the channel to an impulse, i.e., transfer function, can be found via solving the frequency domain equivalent of convection-diffusion (23). Fourier transform of (23) is found by converting the derivative in time domain to multiplication with $j2\pi f$ in frequency domain as

$$j2\pi f\Phi(l, f) = -u\frac{\partial\Phi(l, f)}{\partial l} + D\frac{\partial^2\Phi(l, f)}{\partial l^2} \quad (27)$$

where Φ is the concentration spectral density, which is found by Fourier transform of concentration, i.e., $\Phi = \mathcal{F}\{\phi\}$. Using boundary conditions $\Phi(0, f) = 1$ and $\Phi(\infty, f) = 0$, the transfer function is obtained as

$$H_t(l, \omega) = e^{\left(u\left(1 - \sqrt{1 + \frac{j4\omega D}{u^2}}\right)\frac{l}{2D}\right)} \quad (28)$$

where the temporal frequency f is converted to angular frequency ω using identity $\omega = 2\pi f$. Assuming $|j4\omega D/u^2| < 1$, to have a converging series expansion, $\sqrt{1 + j4\omega D/u^2}$ can be approximated as $1 + j2\omega D/u^2 + 2\omega^2 D^2/u^4$. Finally, we approximate the transfer function as

$$H_t(l, \omega) \approx e^{-\left(\frac{\omega^2 D}{u^3} + j\frac{\omega}{u}\right)l} \quad (29)$$

where we assume $4\omega D/u^2 < 1$ during the derivation, the implication and the practicality of which is further elaborated in Section III-D.

C. Delay

Propagation delay τ for traveling time of peak concentration level $\max_{\tau} \|\phi\|$ to a distance l is found via setting $\partial h(l, \tau)/\partial \tau = 0$ as

$$De^{-\frac{(l-u\tau)^2}{4D\tau}} \frac{(l^2 - \tau(2D + \tau u^2))}{8\sqrt{\pi}(D\tau)^{\frac{5}{2}}} = 0 \quad (30)$$

which yields

$$\tau = \frac{1}{u} \sqrt{\frac{D^2}{u^2} + l^2} - \frac{D}{u^2} \quad (31)$$

The dominance of convection over diffusion is determined by the dimensionless Peclet number (Pe) which is defined as $Pe = ul/D$. For a large value of Pe, the molecular transport is said to be dominated by the convection, and for small Pe values, the transport is dominated by the diffusion. Using definition of Pe number, (31) is rewritten. Furthermore, since the molecular

transport is dominated by the convection, i.e., $Pe \gg 1$, and l is in the order of $\sim 10^{-2}$ m, τ is approximated as

$$\begin{aligned} \tau &= \frac{1}{u} \sqrt{\frac{l^2}{Pe^2} + l^2} - \frac{l}{u} \frac{1}{Pe} \\ &\approx \frac{l}{u} \left(1 + \frac{1}{Pe}\right) \\ &\approx \frac{l}{u} \end{aligned} \quad (32)$$

Since the delay is characterized by the length of the channel l and fluid flow velocity u , we express concentration, and impulse response for microfluidic channels based on distance l . Next, we investigate the spatial frequency response H_s due to translational-invariance apart from temporal frequency response H_t derived previously based on time-invariance.

D. Duality of Transfer Function

Here, we focus on derivation of spatial transfer function H_s and relate it to temporal frequency response H_t . To obtain H_s , we take the Fourier Transform of the impulse response with respect to spatial parameter l as

$$H_s(\nu) = \int_{-\infty}^{\infty} \frac{1}{\sqrt{4\pi D\tau}} e^{-\frac{(l-u\tau)^2}{4D\tau}} e^{-j2\pi\nu l} dl \quad (33)$$

where ν is the spatial frequency and given by $\nu = 1/\lambda$ for a concentration signal with wavelength λ . We obtain transfer function based spatial frequency as

$$H_s(k) = e^{-(k^2 D + jku)\tau} \quad (34)$$

where k is the wave number defined as $k = 2\pi\nu$. The obtained transfer functions based on spatial frequency H_s and temporal frequency H_t , can be converted using the identity

$$\lambda f = u \quad (35)$$

which is the dual of the equality $\lambda f = c$ in electromagnetic waves, where c is the speed of light. Wave number k based on spatial frequency ν is converted to angular frequency ω based on temporal frequency f as

$$k = \frac{\omega}{u} \quad (36)$$

and temporal transfer function H_t can be obtained from spatial transfer function H_s by changing k to ω/u and τ to l/u . We use transfer function based on spatial frequency for analysis of concentration in microfluidic building blocks, and refer it as transfer function H .

During the derivation of the transfer function based on the temporal frequency, we assume $4\omega D/u^2 < 1$, which is related to the Pe as

$$k < \frac{Pe}{4l} \quad (37)$$

In the microfluidic devices, Pe is in the range of $10 < Pe < 10^5$ [31], and the considered distances are in the order of ≈ 10 mm. Therefore, the given upper limit on the frequency, i.e., $Pe/(4l)$, is far beyond the physically achievable frequencies due to the

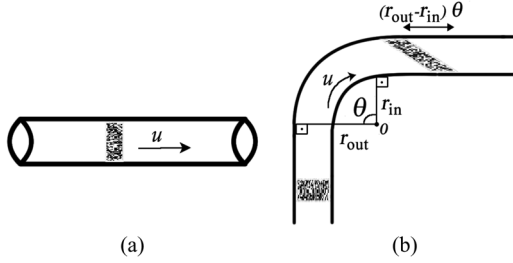


Fig. 3. The building block shapes for straight (a) and turning (b) microfluidic channel configurations.

attenuation, which yields the assumption of $4\omega D/u^2 < 1$ practically meaningful.

IV. MICROFLUIDIC BUILDING BLOCKS AND END-TO-END CONCENTRATION PROPAGATION IN FMC

Closed-form and end-to-end models simplify the analysis and enable efficient-design of molecular communication techniques. In this section, our objective is to obtain the end-to-end concentration propagation model of FMC based on microfluidic building blocks. Therefore, we investigate the channels based on straight and turning configurations, and interconnections based on bifurcation and combining connections.

A. Channel Configurations

Here, we develop end-to-end propagation models for straight and turning channel configurations, which are illustrated in Fig. 3(a) and (b), respectively. To this end, impulse response, delay, and transfer function are determined.

1) *Straight Channels*: Concentration propagation inside straight channel is illustrated in Fig. 3(a). Impulse response of the straight channel is found in (26), here we parametrize it according to channel specific variables as

$$h_{\text{str}}(l) = \frac{1}{\sqrt{4\pi D\tau}} \exp\left(-\frac{(l-u\tau)^2}{4D\tau}\right) \quad (38)$$

where u is the flow velocity in the microfluidic channel, and τ is the delay of the microfluidic channel given by $\tau_{\text{str}} = l/u$. For an input concentration ϕ_+ into straight microfluidic channel, the output concentration ϕ_- can be obtained via convolution of input and impulse response ($h_{\text{str}} * \phi_+$)(l) as

$$\phi_-(l) = \int_{-\infty}^{+\infty} h_{\text{str}}(x)\phi_+(l-x)dx \quad (39)$$

Transfer function of straight channel is derived in (34), and it is parametrized as

$$H_{\text{str}}(k) = e^{-(k^2 D + jku)\tau} \quad (40)$$

Spectrum of the output concentration can be obtained via multiplication of transfer function and input concentration spectrum $\Phi_-(k) = H(k)\Phi_+(k)$.

2) *Turning Channels*: Here, we extend our model for straight channels to turning channels. In Section II-B, we have pointed out the invariance of flow velocity at turning channels in microfluidics [28], [29]. Due to turning, inner and outer radius of the channel are different, which causes different laminas to travel different lengths [32]. Using the linearity property, we calculate propagation of concentration for each lamina using the straight channel model, then add the contribution from each lamina to reach impulse response of the turning channel. The concentration propagation inside the turning microfluidic channel is illustrated in Fig. 3(b), in which turning angle θ , and the radius of the inner and the outer wall of the turning microfluidic channel, i.e., r_{in} and r_{out} , respectively, are depicted as well.

Vertex of θ is defined as the intersection point O of the lines drawn orthogonal to the inner or outer walls at the end of the straight microfluidic channels. Lengths of these drawn lines give radiuses of the the inner or outer wall of the turning microfluidic channel, i.e., r_{in} or r_{out} , based on whether they are drawn orthogonal to the inner or the outer wall, respectively. When circles are drawn using defined inner and outer radiuses with centre point O , the arcs that are subtending angle θ give the inner and outer walls, respectively, of the turning channel which connects two straight microfluidic channels.

We define r_{Δ} as the difference of the radius of the outer and the inner wall of the microfluidic channel as

$$r_{\Delta} = r_{\text{out}} - r_{\text{in}} \quad (41)$$

Using (38), for each lamina in the flow, impulse response is

$$h_{\Delta}(l) = \frac{1}{r_{\Delta}\theta} \frac{1}{\sqrt{4\pi D\tau}} e^{-\frac{(l-u\tau+x')^2}{4D\tau}} \quad (42)$$

where θ is the angle of turn, x' is the change in the traveled path with respect to the axial length l due to turning shape. Contributions from each lamina are integrated and the impulse response for the turning channel is found as

$$h_{\text{turn}}(l) = \frac{1}{r_{\Delta}\theta} \int_{-\frac{r_{\Delta}\theta}{2}}^{\frac{r_{\Delta}\theta}{2}} \frac{1}{\sqrt{4\pi D\tau_{\text{turn}}}} e^{-\frac{(l-u\tau+x')^2}{4D\tau_{\text{turn}}}} dx' \quad (43)$$

where τ_{turn} is taken as the average delay of the laminas in the turning microfluidic channel and is found according to the symmetry around central lamina as $\tau_{\text{turn}} = (l + r_{\Delta}\theta/2)/u$. Impulse response of a turning channel h_{turn} is the same as an ideal integrator with an equivalent axial length straight microfluidic channel

$$h_{\text{turn}}(l) = \left(h_{\text{str}} * \frac{h_{\text{int}}}{r_{\Delta}\theta} \right) (l) \quad (44)$$

where h_{str} is the impulse response of a straight channel having same length with the central arc length of the turning channel, and h_{int} is

$$h_{\text{int}}(l) = \begin{cases} 1, & |l| \leq \frac{r_{\Delta}\theta}{2} \\ 0, & |l| > \frac{r_{\Delta}\theta}{2} \end{cases}$$

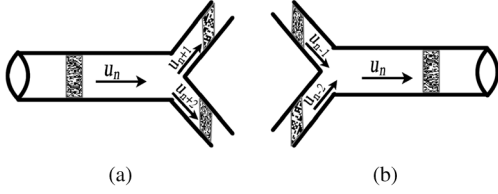


Fig. 4. Building block shapes for bifurcation (a) and combining (b) interconnection configurations.

The transfer function of a turning channel is obtained via Fourier Transform of the (43) as

$$\begin{aligned}
 H_{\text{turn}}(k) &= \int_{-\infty}^{\infty} \frac{1}{r_{\Delta}\theta} \\
 &\cdot \int_{-\frac{r_{\Delta}\theta}{2}}^{\frac{r_{\Delta}\theta}{2}} \frac{1}{\sqrt{4\pi D\tau_{\text{turn}}}} e^{-\frac{(l-u\tau_{\text{turn}}+x')^2}{4D\tau_{\text{turn}}}} dx' e^{-jkl} dl \\
 &= e^{-(k^2 D + jku)\tau_{\text{turn}}} \cdot \frac{\text{sinc}\left(\frac{r_{\Delta}\theta k}{2}\right)}{\frac{r_{\Delta}\theta k}{2}} \quad (45)
 \end{aligned}$$

which is the frequency response of corresponding integrator

$$H_{\text{turn}}(k) = H_{\text{str}}(k)H_{\text{int}}(k) \quad (46)$$

where H_{int} is defined using normalized sinc function as

$$\begin{aligned}
 H_{\text{int}}(k) &= \frac{\text{sinc}\left(\frac{r_{\Delta}\theta k}{2}\right)}{\frac{r_{\Delta}\theta k}{2}} \\
 &= \text{sinc}\left(\frac{r_{\Delta}\theta}{2\pi}k\right) \quad (47)
 \end{aligned}$$

Therefore, turning channel can be seen as an integrator which is a low-pass filter.

Since the obtained impulse response, delay, and transfer function formulations respond to a signal in a future position, we shift them by $r_{\Delta}\theta/2$ to make them causal and obtain the impulse response, delay, and transfer function for turning channel as

$$h_{\text{turn}}(l) = \frac{1}{r_{\Delta}\theta} \int_0^{r_{\Delta}\theta} \frac{1}{\sqrt{4\pi D\tau_{\text{turn}}}} e^{-\frac{(l-u\tau_{\text{turn}}+x')^2}{4D\tau_{\text{turn}}}} dx' \quad (48)$$

where delay is given by $\tau_{\text{turn}} = (l + r_{\Delta}\theta)/u$. Furthermore, shifted transfer function is as

$$H_{\text{turn}}(k) = e^{-(k^2 D + jku)\tau_{\text{turn}}} \text{sinc}\left(\frac{r_{\Delta}\theta}{2\pi}k\right) e^{-jkr_{\Delta}\theta/2} \quad (49)$$

B. Interconnection Configurations

Here, we model concentration propagation for interconnection of multiple channels, which are illustrated in Fig. 4(a) and (b) for bifurcation and combining, respectively. There is no pressure drop and delay in interconnection models. Pressure drop and delay are given by the channels connected to

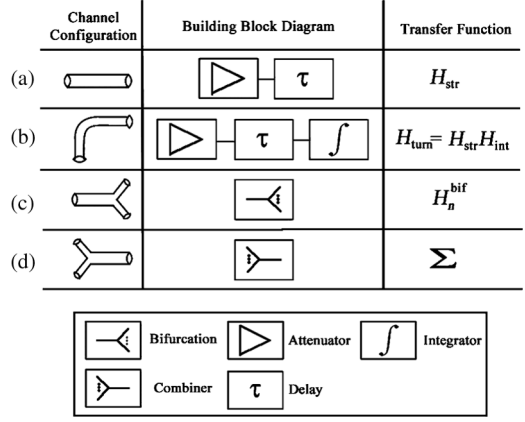


Fig. 5. Building blocks of microfluidic channels for end-to-end molecular transport analysis.

the interconnection node. Overall, we find effect of bifurcation and combining on concentration and spectral density.

1) *Bifurcating Interconnection*: In bifurcating connection, flow is separated proportional to conductance G_n of the diverging microfluidic channels. By conservation of mass, concentration divergence to channels, i.e., ϕ_n^- , from inlet concentration ϕ_+ , is formulated as

$$\phi_n^-(l) = \frac{G_n}{G_{\text{eq}}} \phi_+(l) \quad (50)$$

Similarly, bifurcating channel results in down scale of the output concentration spectral density as

$$\Phi_n^-(k) = \frac{G_n}{G_{\text{eq}}} \Phi_+(k) \quad (51)$$

Therefore we define transfer function of the bifurcating channel as

$$H_n^{\text{bif}} = \frac{G_n}{G_{\text{eq}}} \quad (52)$$

2) *Combining Interconnection*: Combining connection is composed of converging channels. Output concentration ϕ_- is given by the addition of entering concentration from connected channels, i.e., ϕ_n^+ , as

$$\phi_-(l) = \sum_{n=0}^N \phi_n^+(l) \quad (53)$$

Accordingly, output spectrum becomes the addition of the converging concentrations

$$\Phi_-(l) = \sum_{n=0}^N \Phi_n^+(l) \quad (54)$$

C. The End-to-End Model of Concentration Propagation

The end-to-end model is developed using the system-theoretic molecular transport analysis of the microfluidic building blocks, which are summarized in Fig. 5, and provides the impulse response, delay, and transfer function for concentration propagation in FMC.

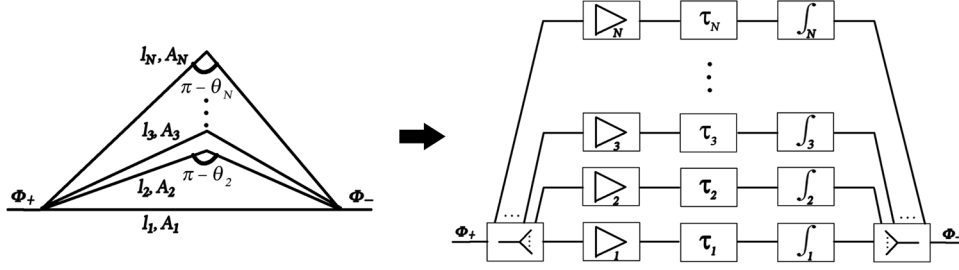


Fig. 6. Microfluidic and building block representation of FIR filter.

End-to-end impulse response of an arbitrary microfluidic circuit h_{e2e} is determined via convolution of the impulse response of each building block as

$$h_{e2e}(l) = (h_1 * h_2 * \dots * h_N)(l) \quad (55)$$

and for a given transmitted molecular concentration, received concentration level is obtained as

$$\phi_-(l) = (h_{e2e} * \phi_+)(l) \quad (56)$$

where ϕ_- and ϕ_+ are received and transmitter concentration levels, respectively. Performed system-theoretic analysis for molecular transport in FMC is also utilized to determine end-to-end propagation delay τ_{e2e} via addition of delay of each building blocks as

$$\tau_{e2e} = \sum_n \tau_n \quad (57)$$

Lastly, the end-to-end transfer function can be determined using performed system-theoretic analysis via multiplying frequency response of building blocks of microfluidic circuit as

$$H_{e2e}(k) = \prod_n H_n(k) \quad (58)$$

and the spectrum of the received molecular concentration is obtained for a given transmitted concentration as

$$\Phi_-(k) = H_{e2e}(k)\Phi_+(k) \quad (59)$$

where Φ_- and Φ_+ are the received and transmitted concentration spectrum, respectively. The developed end-to-end model is used to design microfluidic circuits to yield desired end-to-end transfer function H_{e2e} at the receiver.

V. LEAST-SQUARES FIR FILTERING VIA MICROFLUIDICS

In this section, the utilization of microfluidic channels to create an FIR filter is presented. Specifically, least-squares FIR filtering is used to optimize microfluidic channel parameters according to desired concentration spectral density (CSD).

Suppose we want to design an FIR filter for a given set of frequency domain constraints, i.e., pass and stop bands. For a given constant pressure drop across the microfluidic channels that are first bifurcating then combining as in Fig. 6 between transmitter and receiver, transfer function of individual channels can be adjusted via proper design of length and the cross-section of the channels such that desired FIR filtering operation

can be achieved. To this end, first, we give overview of linear least-squares filter design, then show mapping of channel parameters according to obtained filter coefficients, and we derive the required aspect-ratio of the channel. Lastly, we outline design steps for microfluidic channels, and formulate end-to-end transfer function.

A. Overview of Linear Least-Squares Filter Design

Transfer function of an FIR filter is given by

$$H(k) = \sum_{n=-N}^N \alpha_n e^{-jkn} \quad (60)$$

where $2N + 1$ is the order of the FIR filter. An empirical FIR filtering structure using microfluidic channels is illustrated in Fig. 6. The coefficient sequence α_n is symmetric, i.e., $\alpha_n = \alpha_{-n}$, to have a linear phase filter. The desired frequency response is represented in terms of pass- and stop-bands in the frequency domain $[0, \pi]$. In each pass- and stop-band, the frequency is sampled with k_{sample} spacing, and $M = \pi/k_{\text{sample}}$ is the number of frequencies resulting from frequency domain sampling, such that the frequency response is discretized into M linear equations of the form

$$H(k_m) = \alpha_0 + 2 \sum_{n=1}^N \alpha_n \cos(k_m n) \quad (61)$$

where k_m s are the frequencies whose frequency responses are calculated for $m = 1, \dots, M$. To determine the corresponding filter coefficients to the given desired output concentration spectrum, we define α which contains filter coefficients to be found, \mathbf{z} as the vector containing desired magnitude of the transfer function at frequencies k_m . Overall, state space representation of the system is given as

$$\mathbf{z} \cong \mathbf{\Lambda} \alpha \quad (62)$$

where $\alpha = [\alpha_0, \dots, \alpha_N]^T$, $\mathbf{z} = [H(k_1), \dots, H(k_M)]^T$, and $\mathbf{\Lambda}$ is an M -by- $(N + 1)$ matrix as

$$\mathbf{\Lambda} = \begin{bmatrix} 1 & 2 \cos(k_1) & 2 \cos(2k_1) & \dots & 2 \cos(Nk_1) \\ 1 & 2 \cos(k_2) & 2 \cos(2k_2) & \dots & 2 \cos(Nk_2) \\ \vdots & \vdots & \vdots & \ddots & \vdots \\ 1 & 2 \cos(k_M) & 2 \cos(2k_M) & \dots & 2 \cos(Nk_M) \end{bmatrix} \quad (63)$$

The least-squares optimization problem is formulated as

$$\min_{\alpha} \|\mathbf{\Lambda} \alpha - \mathbf{z}\|_2 \quad (64)$$

which is equivalent to minimizing quadratic error function J defined as

$$J(\boldsymbol{\alpha}) \triangleq \|\mathbf{\Lambda}\boldsymbol{\alpha} - \mathbf{z}\|_2^2 = \boldsymbol{\alpha}^T \mathbf{\Lambda}^T \mathbf{\Lambda} \boldsymbol{\alpha} - \boldsymbol{\alpha}^T \mathbf{\Lambda}^T \mathbf{z} - \mathbf{z}^T \mathbf{\Lambda} \boldsymbol{\alpha} + \mathbf{z}^T \mathbf{z} \quad (65)$$

To minimize J , by taking derivative with respect to $\boldsymbol{\alpha}$ and equating to 0, it is found that

$$\mathbf{\Lambda}^T \mathbf{\Lambda} \boldsymbol{\alpha} = \mathbf{\Lambda}^T \mathbf{z} \quad (66)$$

For a given desired frequency response constraints composed of desired magnitude at pass-band frequency ranges and suppression at stop-band frequency ranges, the FIR filter coefficients can be determined via least-squares method as

$$\boldsymbol{\alpha} = \left[(\mathbf{\Lambda}^T \mathbf{\Lambda})^{-1} \mathbf{\Lambda}^T \right] \mathbf{z} \quad (67)$$

where $\boldsymbol{\alpha}$ contains the obtained filter coefficients via least-squares method. Non-positive α_n values are dropped, as well as non-positive length channels as

$$H(k) = \sum_{n=1}^N \alpha_n e^{-j\beta_n} \quad (68)$$

where $\beta_n = kn$, and linear phase property no longer holds. Obtained filter coefficients, i.e., α_n , and complex exponential exponents, i.e., β_n , are mapped to length and cross-section parameters of microfluidic channels to achieve the desired transfer function between transmitter and receiver in FMC.

B. Length and Area Design of Microfluidic Channels

Here, we map the filter parameters, i.e., α and β , in (68) to microfluidic channel parameters, i.e., length and cross-section area, based on the transfer function of microfluidic building blocks in Fig. 5 and pressure drop constraint Δp . The FIR filter consisting of tapped microfluidic channels in the shape of nested isosceles triangles is depicted in Fig. 6.

The obtained α_n values using least-squares optimization in (67) are normalized due to dropped non-positive values and mapped to the microfluidic channel transfer function (40) as

$$\alpha_n = e^{-k^2 D \tau_n} \quad (69)$$

from which we obtain the desired delay in microfluidic channel n as

$$\tau_n = -\frac{\ln(\alpha_n)}{k^2 D} \quad (70)$$

The complex exponential exponents, i.e., β_n , are mapped using (40) and (68) as

$$\beta_n = k u_n \tau_n \quad (71)$$

Using $l_n = u_n \tau_n$, and $\beta_n = kn$, the required length of the microfluidic channel n is found as

$$l_n = Ln \quad (72)$$

where $n = 1, \dots, N$, and L is defined as the scaling factor for length of the microfluidic channels, i.e. l_n values are calculated as integer multiples of L as $l_n = Ln$. Furthermore, L provides frequency scaling of the overall frequency response of the FIR filter, such that fine-tuning of pass- and stop-band frequencies of the FIR filter can be performed, which is further elaborated via numerical results in Section VI-B.

Using (32), (70), and (72), the required area-averaged flow velocity u_n at the microfluidic channel n is found as

$$u_n = -\frac{k^2 D n}{\ln(\alpha_n)} \quad (73)$$

Furthermore, the cross-section area of the channel must be adjusted accordingly by equating flow velocity u_n to pressure drop constraint Δp_n . Using (15), (22), and (73), required cross-section area is formulated as

$$A_n = -\frac{\ln(\alpha_n) Q_n}{k^2 D n} \quad (74)$$

Next, based on formulated cross-section area of microfluidic channels, we derive required aspect ratio of them.

C. Aspect Ratio Design of Microfluidic Channels

In this section, using (74) and formulated linear conductance relation between Δp and u for rectangular, square, elliptical, and circular cross-sections in Section II-C, required aspect-ratio of microfluidic channels are determined.

1) *Rectangular and Square Cross-Sections*: Using conductance for a rectangular channel G_n^{rect} given in the Table I and (74), we end up with the equality

$$w_n h_n = -\frac{\ln(\alpha_n) h_n^3 w_n \Delta p_n}{12 \mu k^2 D n^2} \left(1 - 0.630 \frac{h_n}{w_n} \right) \quad (75)$$

We define aspect ratio of the rectangular channel as $\gamma = w/h$, and replacing width w with γh , we obtain γ as

$$\gamma_n^{\text{rect}} = \frac{0.63 h_n^2 \Delta p_n}{h_n^2 \Delta p_n + \frac{12 \mu k^2 D n^2}{\ln(\alpha_n)}} \quad (76)$$

Using the determined α_n in (67), for a given height h_n and Δp_n , the channel cross-sections can be designed according to desired filtering operation. Furthermore, for a square channel γ_n is equal to 1, and h_n can be obtained as

$$h_n = \sqrt{-\frac{12 \mu k^2 D n^2}{0.37 \Delta p_n \ln(\alpha_n)}} \quad (77)$$

2) *Elliptical and Circular Cross-Sections*: Using conductance for an elliptical microfluidic channel G_n^{ellps} given in the Table I and area formulation in (74), the following equality is found for cross-section of the microfluidic channel

$$a_n b_n = -\frac{\ln(\alpha_n)}{4 \mu k^2 D n^2} \frac{a_n^3 b_n^3}{a_n^2 + b_n^2} \Delta p_n \quad (78)$$

Aspect ratio of the elliptical microfluidic channel is defined as the ratio of the major axis length to minor axes as $\gamma = a/b$ from which we can obtain desired aspect ratio γ_n^{ellps} as follows

$$\gamma_n^{\text{ellps}} = \sqrt{-\frac{4 \mu k^2 D n^2}{\ln(\alpha_n) b_n^2 \Delta p_n + 4 \mu k^2 D n^2}} \quad (79)$$

For a circular channel radius $r = a = b$, desired radius can be found as

$$r_n = 2 \sqrt{-\frac{2 \mu k^2 D n^2}{\ln(\alpha_n) \Delta p_n}} \quad (80)$$

D. Overview of Microfluidic Channel Design

Here, we summarize the design procedure for microfluidic channels. The calculation of required microfluidic channel length and aspect ratio corresponding the desired frequency response is presented step-by-step.

To form the tapped delay line FIR filter via linear least-squares filtering, overall design procedure can be grouped under three main steps as follows

- 1) From the given desired pass and stop bands of the frequency response, the channel design problem is formulated as a least-squares FIR filtering problem as presented in (62).
- 2) From the formulated least-squares problem, required α and β values are determined for each microfluidic channel to be mapped to microfluidic channel parameters.
- 3) Obtained α and β values enable the design of a tapped delay line filter using microfluidic channels. Length and cross-section aspect ratio of channels are designed according to the found α and β , and the given cross-section shape and pressure-drop between the transmitter and the receiver.

The output spectrum of the devised microfluidic FIR filter is given by

$$\begin{aligned} \Phi_{-}(k) &= \sum_{n=1}^N H_n^{\text{str}}(k) H_n^{\text{int}}(k) \Phi_{+}(k) \\ &= \sum_{n=1}^N e^{-k^2 D \tau_n} e^{-jk L n} \text{sinc} \left(\frac{r_n^{\Delta} \theta_n}{2\pi} k \right) \Phi_{+}(k) \quad (81) \end{aligned}$$

where H_n^{str} is the transfer function of the microfluidic channel n with the length l_n , the aspect ratio γ_n , and the pressure drop Δp_n ; H_n^{int} is the transfer function of the turn n with the angle $\theta_n = \pi - 2 \arcsin(l_1/(2l_n))$, and the difference of inner and outer radius r_n^{Δ} .

This concludes our discussion on design of microfluidic circuits. Next, we present numerical results, and discuss the accuracy and practical issues regarding the performance of the microfluidic channel design.

VI. NUMERICAL RESULTS

In this section, we, first, study the transfer functions developed for FMC in microfluidic channels. Specifically, we investigate the effect of channel cross-section and length for straight channels, and effect of turning angle θ and difference of inner and outer turning radius r_{Δ} for turning channels. Then, example design of band-pass and band-stop filters via least-squares FIR filtering are presented for FMC. During numerical evaluations, viscosity μ of the fluid is set to 10^{-3} Pa·s, and diffusion constant D is set to $10 \cdot 10^{-10}$ m²/s. Furthermore, the results presented in Fig. 7–10 with respect to the wave number k can be converted to the angular frequency ω using the identity given in (36).

A. Concentration Propagation

The concentration propagation is studied in two parts, i.e., straight and turning channels. For straight channels with rectangular, square, elliptical, and circular cross-sections, transfer

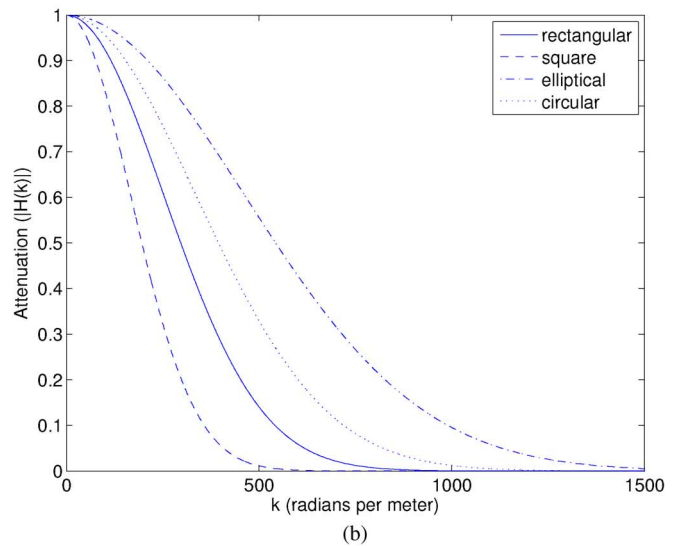
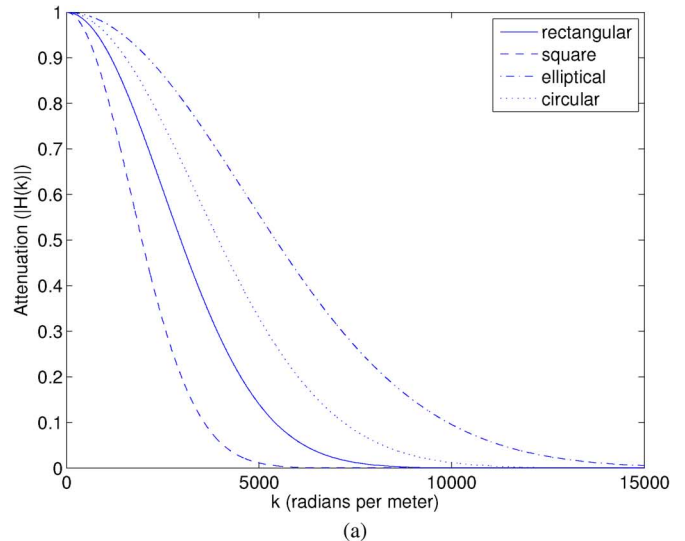


Fig. 7. Attenuation of the concentration propagation in the straight channel. The magnitude of the transfer functions with different cross-sections against wave number k , for the channel lengths of 10 mm and 100 mm in (a) and (b), respectively.

function is investigated for channel length l of 10 and 100 mm. For turning channels with varying turn angles θ , the transfer function is investigated for inner and outer radius differences r_{Δ} of 50 and 100 μm . The pressure drop Δp across channels is set to 500 Pa.

1) *Straight Channel:* For rectangular channels, height is $h = 6 \mu\text{m}$ and width is $w = 25 \mu\text{m}$. For the square microfluidic channels, height is $h = 6 \mu\text{m}$. For the elliptical microfluidic channels, major axis radius is $a = 25 \mu\text{m}$, minor axis radius is $b = 6 \mu\text{m}$. For circular channel, radius is $r = 6 \mu\text{m}$. Results for channel length $l = 10$ mm and 100 mm are presented in Fig. 7. The corresponding flow velocities u are tabulated in the Table II.

The concentration signals with higher frequency can be transported with less attenuation between a transmitter and receiver pair in the elliptical and the circular channels compared to the rectangular and the square channels. When the channel length is increased from 10 mm to 100 mm, the achievable frequencies

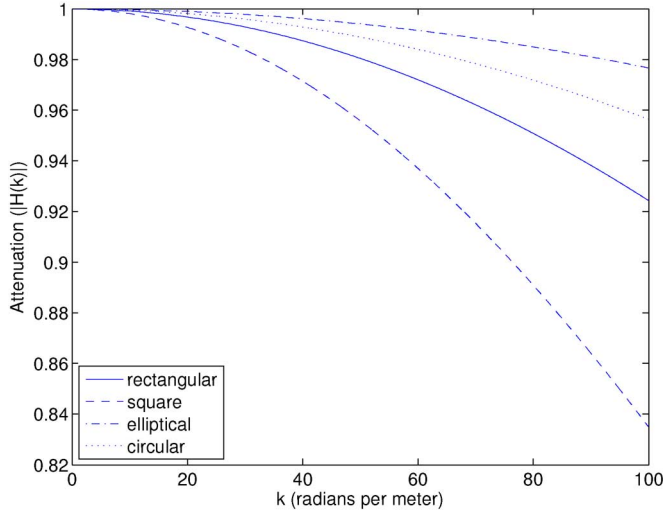


Fig. 8. Attenuation of the concentration propagation for a low range of frequencies representing the spectrum of interest for the bacteria-based biological oscillator applications. The magnitude of the transfer functions with different cross-sections against the wave number k , for a straight channel with a length of 100 mm.

are decreased in the order of 10 from Fig. 7(a) to (b). The achievable frequencies in the channels are inversely scaled by the rate of increase in the distance between transmitter and receiver.

The presented results in Fig. 7 for attenuation can be utilized to assess performance of the MC among different bacteria populations in the microfluidic channels. A biological oscillator development is performed in [33] based on the quorum sensing, where the period of concentration signal is in the order of minutes and even hours, i.e., the frequency of the signal is in the order of 10^{-2} and 10^{-4} s $^{-1}$. Accordingly, the attenuation of concentration is presented in the Fig. 8 for the low range of frequencies, i.e., up to $k = 100$ radians per meter which is equal to the temporal frequency of $f = 2.02 \cdot 10^{-4}$, $8.83 \cdot 10^{-5}$, $6.76 \cdot 10^{-4}$, and $3.58 \cdot 10^{-4}$ s $^{-1}$ for rectangular, square, elliptic, and circular channels, respectively. It is observed in Fig. 8 that for the frequencies below 10 radians per meter, attenuation in the microfluidic channels becomes negligible.

2) *Turning Channel*: The turning channel results for rectangular channels are presented in Fig. 9. The channel height h is taken to be 10 μm , width w is taken as 50 μm , and channel length is 5 mm. The inner and outer radius differences of $r_{\Delta} = 50$ and 100 μm are used. The turning angle θ is selected as $\pi/3$, $3\pi/4$, $5\pi/6$, and π .

As the turning angle increases from $\pi/3$ to π , achievable frequencies in the turning channel decreases. When the inner and outer radius of turn r_{Δ} is increased from 50 to 100 μm , achievable frequencies decrease for the same channel length in Fig. 9(a) and (b), respectively. Furthermore, the achievable frequencies in the channels is adversely effected by increasing turning angle, and this effect is further amplified for higher r_{Δ} .

The frequency response becomes 0 when the wave number k is a positive integer i multiple of the reciprocal of the difference of the traveled paths by the outermost lamina and the innermost lamina, i.e., $1/(r_{\Delta}\theta)$, as

$$k = \frac{1}{r_{\Delta}\theta} i \quad (82)$$

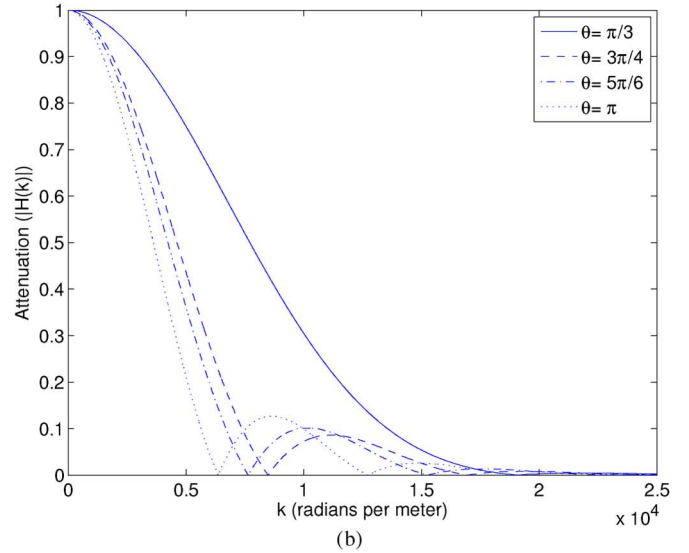
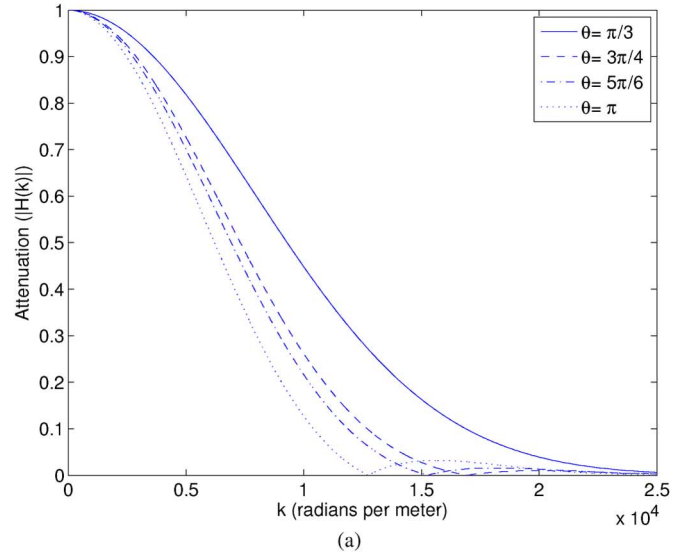


Fig. 9. Attenuation of concentration propagation in turning channel. The magnitude of the transfer functions with different turning angles against wave number k , for radius difference of 50 and 100 μm in (a) and (b), respectively.

This effect is peculiar to the concentration propagation in turning microfluidic channels, and it is due to the addition of phase shifted lamina that cancel out the frequency components given by (82) at the output signal. From the mathematical point of view, the turning channel performs integration of the input signal, and since integration of a sinusoidal signal over a complete period, or multiple complete periods would yield 0, frequency components matching this definition vanish, which are characterized in (82).

B. Microfluidic FIR Filtering

Here, we present two example designs of microfluidic channels for FIR filtering in FMC. The FIR filter structure is illustrated in Fig. 6. The value of N is set to 10. Pressure drop across channels is set to $\Delta P = 100$ Pa. The rectangular channels are used for design. The height of channels is selected as $h = 5$ μm . The width w of channels is determined according to desired aspect ratio based on the filter constraints. The difference of inner and outer radius at turn is taken as $r_{\Delta} = 5$ μm . In each stop and

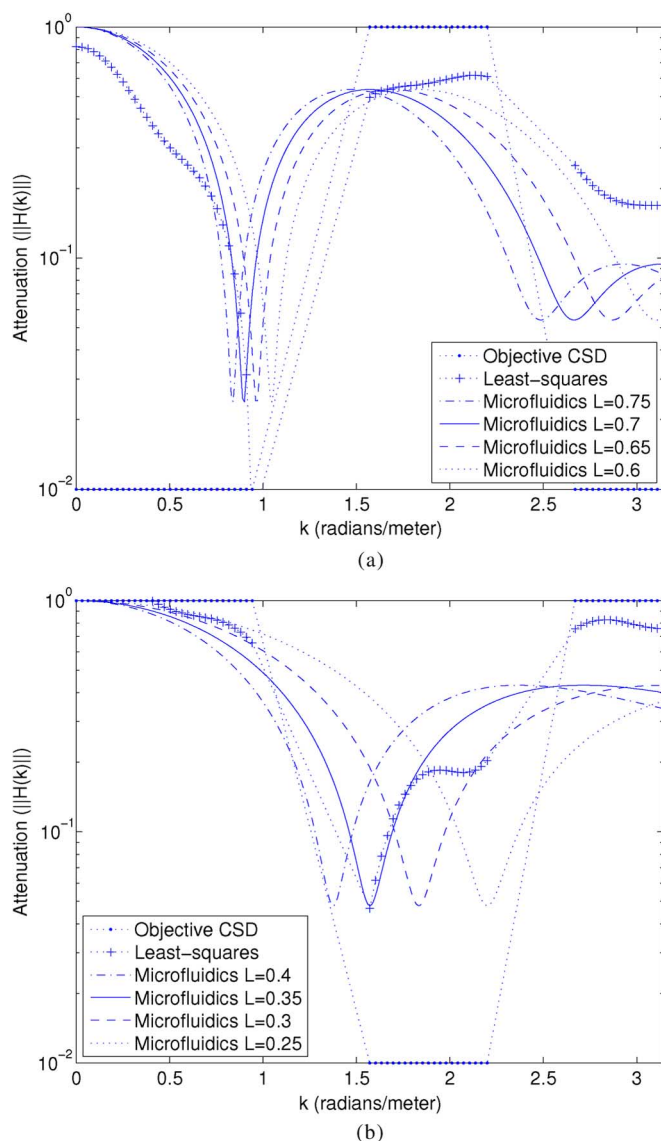


Fig. 10. The frequency response of devised band-pass (a) and band-stop (b) filters.

TABLE II

SUMMARY OF FLOW VELOCITIES (u) IN DIFFERENT CHANNEL CROSS-SECTIONS

Cross-section	$l = 10 \cdot 10^{-3} \text{ m}$	$l = 100 \cdot 10^{-3} \text{ m}$
Rectangular	$1.27 \cdot 10^{-4} \text{ m/s}$	$1.27 \cdot 10^{-5} \text{ m/s}$
Square	$5.55 \cdot 10^{-5} \text{ m/s}$	$5.55 \cdot 10^{-6} \text{ m/s}$
Elliptical	$4.25 \cdot 10^{-4} \text{ m/s}$	$4.25 \cdot 10^{-5} \text{ m/s}$
Circular	$2.25 \cdot 10^{-4} \text{ m/s}$	$2.25 \cdot 10^{-5} \text{ m/s}$

pass band, the frequency is sampled with 0.01 spacing. Magnitude in pass bands is set to 1, and suppression amount in stop bands is set to 10^{-2} . After least-squares optimization of filter coefficients α_n , only positive coefficients are used for channel design. Branches of filter with non-positive coefficient are removed, i.e., α_n is set to 0 for those channels. For aspect ratio design, k in (76) is set to π . Results for band-pass and band-stop filtering are presented in Fig. 10.

The band-pass filter has one pass band, i.e., $0.5\pi-0.7\pi$, and two stop bands, i.e., $0-0.3\pi$ and $0.85\pi - \pi$. The objective frequency response of the band-pass filter and its least-squares ap-

proximation are presented in Fig. 10(a). For band-pass filtering, the effect of scaling factor L is studied for $L = 0.75, 0.7, 0.65$, and 0.5 . The band-stop filter has one stop band, i.e., $0.5\pi-0.7\pi$, and two pass bands, i.e., $0-0.3\pi$ and $0.85\pi - \pi$. The objective frequency response of the band-stop filter and its least-squares approximation are presented in Fig. 10(b). For band-stop filtering, the effect of scaling factor L is studied for $L = 0.4, 0.35, 0.3$, and 0.25 . Transfer function of the devised microfluidic FIR filter can be fine-tuned to a desired pass and stop bands via adjusting L appropriately. Magnitude of the frequencies in the received CSD can be controlled, and the unwanted frequencies can be suppressed by placing the devised microfluidic FIR filter between the transmitter and the receiver patches, such as a biological oscillator based on bacteria population [33].

VII. CONCLUSIONS

In this paper, system-theoretic analysis and least-squares design of microfluidic channels are performed for Flow-induced Molecular Communications (FMC). The objective of this work is the development of end-to-end concentration propagation model based on microfluidic channel configurations, i.e., building blocks of FMC. To the best of our knowledge, this is the first study of concentration propagation in FMC. Furthermore, using the developed system-theoretic end-to-end model for building blocks of FMC, the Finite Impulse Response (FIR) filters are devised. Specifically, the least-squares method is used to map channel parameters to the desired FIR filter frequency response. A parallel connection of microfluidic channels scheme is proposed similar to tapped delay lines. The transfer functions of straight and turning channels are investigated for various length and turning angles, and example design of microfluidic channels are presented for band-pass and band-stop filtering of concentration signal.

REFERENCES

- [1] I. F. Akyildiz, J. M. Jornet, and M. Pierobon, "Nanonetworks: A new frontier in communications," *Commun. ACM*, vol. 54, no. 11, pp. 84–89, Nov. 2011.
- [2] I. F. Akyildiz, F. Brunetti, and C. Blazquez, "Nanonetworks: A new communication paradigm," *Comput. Netw. J. (Elsevier)*, vol. 52, no. 12, pp. 2260–2279, Aug. 2008.
- [3] B. Atakan and O. B. Akan, "On channel capacity and error compensation in molecular communication," *Springer Trans. Computat. Syst. Biol.*, vol. 10, pp. 59–80, Dec. 2009.
- [4] M. Pierobon and I. F. Akyildiz, "End-to-end physical model of molecular communications," *IEEE J. Sel. Areas Commun.*, vol. 28, no. 4, pp. 602–611, May 2010.
- [5] J. Atencia and D. J. Beebe, "Controlled microfluidic interfaces," *Nature*, vol. 437, no. 7059, pp. 648–655, Sep. 2005.
- [6] G. M. Whitesides, "The origins and the future of microfluidics," *Nature*, vol. 442, no. 7101, pp. 368–373, Jul. 2006.
- [7] I. F. Akyildiz, F. Fekri, R. Sivakumar, C. R. Forest, and B. K. Hamner, "MONACO Fundamentals of molecular nano-communication networks," *IEEE Wireless Commun.*, vol. 19, no. 5, pp. 12–18, Oct. 2012.
- [8] B. Atakan and O. B. Akan, "Deterministic capacity of information flow in molecular nanonetworks," *Nano Commun. Netw. J. (Elsevier)*, vol. 1, no. 1, pp. 31–42, Mar. 2010.
- [9] M. Pierobon and I. F. Akyildiz, "Diffusion-based noise analysis for molecular communication in nanonetworks," *IEEE Trans. Signal Process.*, vol. 59, no. 6, pp. 2532–2547, Jun. 2011.
- [10] M. Pierobon and I. F. Akyildiz, "Noise analysis in ligand-binding reception for molecular communication in nanonetworks," *IEEE Trans. Signal Process.*, vol. 59, no. 9, pp. 4168–4182, Sep. 2011.
- [11] M. Pierobon and I. F. Akyildiz, "Capacity of a diffusion-based Molecular communication system with channel memory and molecular noise," *IEEE Trans. Inf. Theory*, vol. 59, no. 2, pp. 942–954, Feb. 2013.

- [12] T. Nakano and J.-Q. Liu, "Design and analysis of molecular relay channels: An information theoretic approach," *IEEE Trans. Nanobiosci.*, vol. 9, no. 3, pp. 213–221, Sep. 2010.
- [13] K. W. Oh, K. Lee, B. Ahn, and E. P. Furlani, "Design of pressure-driven microfluidic networks using electric circuit analogy," *Lab Chip*, vol. 12, no. 3, pp. 515–545, Feb. 2012.
- [14] Y. Wang, T. Mukherjee, and Q. Lin, "Systematic modeling of microfluidic concentration gradient generators," *J. Micromechan. Microeng.*, vol. 16, no. 10, pp. 2128–2137, Sep. 2006.
- [15] Y. Zhou, Y. Wang, T. Mukherjee, and Q. Lin, "Generation of complex concentration profiles by partial diffusive mixing in multi-stream laminar flow," *Lab Chip*, vol. 9, no. 10, pp. 1439–1448, 2009.
- [16] S. K. Griffiths and R. H. Nilson, "Design and analysis of folded channels for chip-based separations," *Anal. Chem.*, vol. 74, no. 13, pp. 2960–2967, Jul. 2002.
- [17] S. K. Griffiths and R. H. Nilson, "Low-dispersion turns and junctions for microchannel systems," *Anal. Chem.*, vol. 73, no. 2, pp. 272–278, Jan. 2001.
- [18] A. S. Bedekar, Y. Wang, S. Krishnamoorthy, S. S. Siddhaye, and S. Sundaram, "System-level simulation of flow-induced dispersion in lab-on-a-chip systems," *IEEE Trans. Comput.-Aided Des. Integr. Circuits Syst.*, vol. 25, no. 2, pp. 294–304, Feb. 2006.
- [19] Y. Xie, Y. Wang, L. Chen, and C. H. Mastrangelo, "Fourier microfluidics," *Lab Chip*, vol. 8, no. 5, pp. 779–785, May 2008.
- [20] E. De Leo, L. Galluccio, A. Lombardo, and G. Morabito, "Networked Labs-on-a-Chip (NLoC): Introducing networking technologies in microfluidic systems," *Nano Commun. Netw. (Elsevier)*, vol. 3, no. 4, pp. 217–228, Dec. 2012.
- [21] H. Bruus, *Theoretical Microfluidics*. Oxford, U.K.: Oxford Univ. Press, 2008.
- [22] B. Kirby, *Micro- and Nanoscale Fluid Mechanics: Transport in Microfluidic Devices*. New York: Cambridge Univ. Press, 2010.
- [23] J. M. Koo and C. Kleinstreuer, "Liquid flow in microchannels: Experimental observations and computational analyses of microfluidics effects," *J. Micromech. Microeng.*, vol. 13, no. 5, pp. 568–579, May 2003.
- [24] D. Di Carlo, "Inertial microfluidics," *Lab Chip*, vol. 9, no. 21, pp. 3038–3046, Nov. 2009.
- [25] D. Huh, J. H. Bahng, Y. B. Ling, H. H. Wei, O. D. Kripfgans, J. B. Fowlkes, J. B. Grotberg, and S. Takayama, "Gravity-driven microfluidic particle sorting device with hydrodynamic separation amplification," *Anal. Chem.*, vol. 79, no. 4, pp. 1369–1376, Feb. 2007.
- [26] D. Di Carlo, D. Irimia, R. G. Tompkins, and M. Toner, "Continuous inertial focusing, ordering, and separation of particles in microchannels," *Proc. Natl. Acad. Sci. USA*, vol. 104, no. 48, pp. 18892–18897, Nov. 2007.
- [27] M. J. Fuerstman, P. Deschatelets, R. Kane, A. Schwartz, P. J. A. Kenis, J. M. Deutch, and G. M. Whitesides, "Solving mazes using microfluidic networks," *Langmuir*, vol. 19, no. 11, pp. 4714–4722, Apr. 2003.
- [28] S. Gendels and A. Jakovics, "Numerical modeling of hydraulic resistance in pipes of various shapes," *Latvian J. Phys. Tech. Sci.*, vol. 41, no. 4, pp. 13–27, 2004.
- [29] A. Brask, G. Goranovic, and H. Bruus, "Theoretical analysis of the low-voltage cascade electro-osmotic pump," *Sens. Actuat. B: Chem.*, vol. 92, no. 1–2, pp. 127–132, Jul. 2003.
- [30] D. Dutta, A. Ramachandran, and D. T. Leighton, Jr., "Effect of channel geometry on solute dispersion in pressure-driven microfluidic systems," *Microfluid. Nanofluid.*, vol. 2, no. 2, pp. 275–290, July 2006.
- [31] H. A. Stone, A. D. Stroock, and A. Ajdari, "Engineering flows in small devices: Microfluidics toward a lab-on-a-chip," *Ann. Rev. Fluid Mech.*, vol. 36, pp. 381–411, Jan. 2004.
- [32] J. I. Molho, A. E. Herr, B. P. Mosier, J. G. Santiago, and T. W. Kenny, "Optimization of turn geometries for microchip electrophoresis," *Analyt. Chem.*, vol. 73, no. 6, pp. 1350–1360, Mar. 2001.
- [33] T. Danino, O. Mondragon-Palomino, L. Tsimring, and J. Hasty, "A synchronized quorum of genetic clocks," *Nature*, vol. 463, no. 7279, pp. 326–330, Jan. 2010.



A. Ozan Bicen (S'08) received the B.Sc. and M.Sc. degrees in electrical and electronics engineering from Middle East Technical University, Ankara, Turkey, in 2010 and from Koc University, Istanbul, Turkey, in 2012, respectively.

He is currently a Graduate Research Assistant in the Broadband Wireless Networking Laboratory and pursuing his Ph.D. degree at the School of Electrical and Computer Engineering, Georgia Institute of Technology, Atlanta. His current research interests include design and analysis of molecular communication systems, cognitive radio networks, and wireless sensor networks.



Ian F. Akyildiz (M'86–SM'89–F'96) received the B.S., M.S., and Ph.D. degrees in computer engineering from the University of Erlangen-Nuremberg, Germany, in 1978, 1981, and 1984, respectively.

Currently, he is the Ken Byers Chair Professor in Telecommunications with the School of Electrical and Computer Engineering, Georgia Institute of Technology (Georgia Tech), Atlanta, the Director of the Broadband Wireless Networking Laboratory and Chair of the Telecommunication Group at Georgia Tech. His current research interests are in

nanonetworks, Long Term Evolution (LTE) advanced networks, cognitive radio networks and wireless sensor networks.

Dr. Akyildiz is an honorary professor with the School of Electrical Engineering at Universitat Politècnica de Catalunya (UPC), Barcelona, Catalunya, Spain, and founded the N3Cat (NaNoNetworking Center in Catalunya). He is also an honorary professor with the Department of Electrical, Electronic and Computer Engineering at the University of Pretoria, South Africa, and the founder of the Advanced Sensor Networks Lab. Since September 2012, he has also been a FiDiPro Professor (Finland Distinguished Professor Program (FiDiPro) supported by the Academy of Finland) at Tampere University of Technology, Department of Communications Engineering, Finland. He is the Editor-in-Chief of *Computer Networks* (Elsevier) journal, and the founding Editor-in-Chief of the *Ad Hoc Networks* (Elsevier) journal, the *Physical Communication* (Elsevier) journal, and the *Nano Communication Networks* (Elsevier) journal. He is an ACM Fellow (1997). He received numerous awards from IEEE and ACM.